Navigational Use of Cassini ΔV Telemetry

Duane C. Roth[*], Peter G. Antreasian[†], Shadan M. Ardalan[†], Kevin E. Criddle[†], Troy Goodson[*], Rodica Ionasescu[†], Jeremy B. Jones[*], Daniel W. Parcher[†], Frederic J. Pelletier[*], Paul F. Thompson[*], and Andrew T. Vaughan[†]
Jet Propulsion Laboratory, California Institute of Technology, Pasadena, CA, 91109

Telemetry data are used to improve navigation of the Saturn orbiting Cassini spacecraft. Thrust induced ΔV's are computed on-board the spacecraft, recorded in telemetry, and downlinked to Earth. This paper discusses how and why the Cassini Navigation team utilizes spacecraft ΔV telemetry. Operational changes making this information attractive to the Navigation Team will be briefly discussed, as will spacecraft hardware and software algorithms responsible for the on-board computation. An analysis of past ΔV telemetry, providing calibrations and accuracies that can be applied to the estimation of future ΔV activity, is described.

Nomenclature

$\Delta \boldsymbol{V}$ = change in velocity
Δt = time since last accelerometer reading
μ_m = mean value of samples
σ = standard deviation
τ_R = rise-time constant before reaching steady-state thrust
τ_F = thrust tail-off time constant after valve closure
ETOX = transformation matrix from International Celestial Reference Frame to spacecraft coordinates
f_m = probability density function
k_{bias} = accelerometer bias
k_{sf} = accelerometer scale factor
L_m = likelihood function
m = spacecraft mass
R = roll rotation matrix
STOI = transformation matrix from spacecraft coordinates to an intermediate coordinate system
T = steady-state thruster force
TURN = offset turn rotation matrix
$\boldsymbol{u}$ = unit thrust vector direction
w = thrust pulse width
x = measurement sample
Y = yaw rotation matrix
$z_{pre\text{-}aim}$ = projection of the initial Main Engine (ME) thrust unit vector onto the accelerometer sensing axis
Δz = projection of the ME gimbal angle about the pre-aim vector onto the accelerometer sensing axis

I. Introduction

CASSINI-HUYGEN'S extremely successful prime mission was completed on July 1, 2008 after nearly eleven years of spacecraft flight operations and four years of Saturn orbital operations. Operational highlights of the joint National Aeronautics and Space Administration/European Space Agency/Italian Space Agency mission include the release and landing of the Huygens probe onto the surface of Saturn's largest moon, Titan, and the completion of 45 Titan and 7 icy satellite targeted encounters within 75 revolutions of Saturn. The Cassini-Huygens mission enabled several exciting discoveries, including lakes on Titan, ice volcanoes on Saturn's smaller moon, Enceladus, and an equatorial mountain range on Saturn's outermost large moon, Iapetus. The mission has added immensely to the understanding of the composition and structure of Saturn's atmosphere, magnetosphere, rings, and satellites.

[*] Member of the Technical Staff, Guidance, Navigation, and Control Section, Mail Stop 230-205, AIAA Member.
[†] Member of the Technical Staff, Guidance, Navigation, and Control Section, Mail Stop 230-205.

Navigation is an essential component to achieving these and other science objectives. With guidelines provided by project scientists, the navigation process begins with development of a mission reference trajectory[1-3] that optimizes science information returned from the twelve orbiter instruments.[4] The reference trajectory is occasionally updated as estimates of satellite orbits and gravity fields improve and to better satisfy science objectives. Radio-metric tracking data and optical navigation images are collected and input into the orbit determination process in order to determine the actual spacecraft orbit[5-7] and maneuvers are then designed and executed to adjust the orbit according to the reference trajectory.[8-11] The maneuver targeting strategy constrains orbit deviations near close encounters while allowing larger deviations away from close encounters.[12] In this manner, accurate gravity assists are achieved and downstream propellant usage is reduced. For the prime mission, 400 m/s of propellant ΔV was used to leverage 33 km/s of gravity assist ΔV. Science observations were also well served by constraining trajectory deviations near satellite encounters. Many observations are sensitive to pointing errors, and because science observations are designed using the reference trajectory instead of the actual operational trajectory, small trajectory deviations near close encounters lead to small pointing errors. The observation target range is typically large away from targeted close encounters, so pointing errors typically remain small away from close encounters. Occasionally, trajectory deviations are large enough that a science observation may be degraded. In these cases, a late pointing or timing update is applied to the sequence of commands enabling the observation. The update is based upon an operational predicted trajectory instead of the reference trajectory. As they require tight turnaround times and impact workforce, the number of late updates must be balanced against economical and other operational considerations.

To improve the accuracy of both predicted and reconstructed trajectories, the navigation team obtains telemetry data consisting of time-tagged on-board ΔV computations from past spacecraft thrust events and includes this information in the implementation of dynamical models and in the initialization of filter parameters used in the estimation process. Thruster on-times and accelerometer counts collected aboard the spacecraft are coupled with spacecraft-relative thruster orientation and spacecraft inertial attitude information to compute ΔV values in International Celestial Reference Frame (ICRF)[13] coordinates. Reconstruction of Orbit Trim Maneuvers (OTMs) benefit from the directional information contained within the downlinked ΔV vector. The many maneuvers performed during the four-year tour provide a database from which right ascension (RA) and declination accuracies can be statistically characterized. Reconstruction of non-maneuver thruster events executed in the blind (without tracking coverage) benefit from the magnitude information. ΔVs directed along the Earth-line while tracking, routinely scheduled during tour operations in order to bias the spacecraft's Reaction Wheel Assembly (RWA), are very accurately reconstructed from radio-metric tracking data and provide a calibration of ΔV magnitude derived from telemetry. Ardalan et al.[14] provides a more comprehensive description of non-maneuver activities involving thrusters and generally complements the discussion contained herein. Whereas there is some overlap in reporting, ref. 14 focuses primarily on operations processes whereas this report focuses primarily on derivation of telemetry accuracies.

II. Telemetry Utilization History and Overview

Cassini telemetry has included ΔV information since launch of the spacecraft in October 1997, but it was not used extensively in navigation operations until May 2005. Prior to this date, utilization was restricted to assistance with the reconstruction of the Saturn Orbit Insertion (SOI) maneuver. Reasons for neglecting it were two-fold: its resolution was very poor and accurate characterization and calibration sources were unavailable. Because targeting requirements were less stringent during cruise, no action was taken to remedy these conditions. With long flight times and less orbital dynamics between targets, there was less sensitivity to miss distances from targets.

The resolution of ΔV telemetry was poor prior to May 2005 because it was configured to prevent saturation of counters during large maneuvers such as the 450 m/s Deep Space Maneuver (DSM), 627 m/s SOI, and the 393 m/s Periapsis Raise Maneuver (PRM). Poor resolution coupled with the chosen attitude control mode prevented the calibration of non-maneuver thruster events during cruise phase. Cassini's attitude was typically maintained using the Reaction Control System (RCS), conserving RWA consumables for Saturn orbital operations. RCS mode employs a set of eight 1-newton thrusters, four coupled and four uncoupled. Thrusters fired approximately every two hours to maintain the attitude within the designated deadband limit. The resulting ΔVs were frequent and small, smaller than the resolving capability of telemetry.

Fewer maneuvers and less accurate reconstructions prevented the statistical characterization of ΔV telemetry associated with cruise phase maneuvers. A sample size of eighteen maneuvers, fifteen using the 440 newton main engine (ME) and three using the RCS, was too small to provide reliable results. In addition, less orbital dynamics, more frequent attitude control thrusting, and larger solar pressure induced spacecraft acceleration uncertainties significantly reduced maneuver reconstruction accuracies.

Maneuver sample size increased significantly in tour operations, with a maneuver executed every two weeks on average since capture into orbit around Saturn. Reconstructed maneuver accuracies improved significantly after entering into orbit around Saturn because the short 8 to 48 day orbital periods imparted much more signature onto the collected radio-metric data types. In addition, spacecraft attitude changes became managed primarily with reaction wheels instead of thrusters, as RWA mode provides a significantly more stable platform for science observations. Rather than firing thrusters every two hours as deadband limits were approached, thrusters fired every few days to maintain reaction wheel speeds within operational specifications. Fewer orbit perturbations resulted in more isolated maneuver events, allowing them to be reconstructed more accurately. Also, solar pressure uncertainties became significantly smaller at Saturn's solar distance, further improving navigational accuracies.

With regard to the aforementioned changes brought about in tour operations, the utilization of on-board ΔV computations was re-evaluated and found to hold potential for further improvement of navigation operations. To realize benefits, an increase in resolution was required. Shortly after the January 2005 Huygens probe landing onto the surface of Titan, resources were freed to pursue a flight software update that would improve the efficiency of Saturn orbital operations. One goal of this update was to modify ΔV scale factors in order to increase resolution. Upon activation of AACS FSW A8.7.2 in late May 2005, the size of the minimum per-axis ΔV increment, or Data Number (DN), written into telemetry was reduced from 2 mm/s to 0.04 mm/s. Telemetry from this date onward was evaluated and calibrated.

Fundamental differences exist between on-board ΔV computations for uncoupled RCS thrusting and those for ME thrusting. From ref. 15, ΔV's associated with RCS thrusting are computed according to

$$\Delta \boldsymbol{V} = \sum_{i=1}^{n} \frac{\left[w_i + (1 - e^{-w_i/\tau_R})(\tau_F - \tau_R) \right] T}{m} \boldsymbol{u}_i \tag{1}$$

where n is the number of uncoupled pulses, w the thrust pulse width, τ_R the exponential rise-time constant before reaching steady-state thrust, τ_F the exponential thrust tail-off time constant after valve closure, T the steady-state thruster force, m the spacecraft mass, and $\boldsymbol{u}$ is the unit thrust vector direction in ICRF coordinates. The parameters τ_R, τ_F, m, and T are commanded parameters within the spacecraft flight software and are regularly updated. The parameters w and $\boldsymbol{u}$ are global variables available to flight software. The parameter n accumulates until counters are either reset or saturated. RCS maneuvers are terminated via a "virtual accelerometer" – effectively a timer, so that the reported maneuver magnitude is the same as the requested magnitude. Accuracies are almost entirely dependent on the accuracy of T loaded in flight software. Thruster rise and tail-off time constants do not significantly impact RCS maneuver ΔV computations because they are much shorter than the thrust pulse widths. Spacecraft mass one-sigma uncertainties are less than 0.5%.

Delta-V's associated with ME thrust are computed according to

$$\Delta \boldsymbol{V} = \sum_{i=1}^{n} \frac{k_{sf} \times \Delta V_{DNi} - k_{bias} \times \Delta t_i}{z_{pre\text{-}aim} + \Delta z_i} \boldsymbol{u}_i \tag{2}$$

where n is the number of spacecraft real-time increments (RTI's) elapsed during the measurement, ΔV_{DN} the data number reported by the accelerometer, k_{sf} a scale factor to convert from DN to meters per second, k_{bias} the accelerometer bias, Δt the time since the last accelerometer reading, $\boldsymbol{u}$ the unit thrust vector direction, $z_{pre\text{-}aim}$ the projection of the initial ME thrust unit vector onto the accelerometer sensing axis (equal to approximately cosine 6°), and Δz is the projection of the ME gimbal angle about the pre-aim vector onto the accelerometer sensing axis. The parameters k_{sf} and $z_{pre\text{-}aim}$ are commanded, whereas $\boldsymbol{u}$, ΔV_{DN}, Δt, and Δz are global variables. The parameter k_{bias} is computed on-board the spacecraft during a quiescent period after the accelerometer is powered on and before maneuver execution.[16]

III. Calibration and Evaluation

Before telemetered ΔV information can be implemented into the navigation process, an understanding of its accuracy must be established. Accuracy estimates are obtained by comparing telemetry computations to navigation team reconstructions of maneuvers and other ΔV activity. The reconstructions are based on a weighted, least squares fit of Doppler, range, and optical navigation images over arc lengths spanning 1.5 revolutions or more about Saturn. Telemetry information is discarded for these particular reconstructions in order to maintain independent ΔV

estimates. For maneuvers, *a priori* information consists of the nominal maneuver design and constraints derived from maneuver execution error model 2007-02.[17]

For non-maneuver ΔV activities, *a priori* information is irrelevant because estimates are driven entirely by radio-metric tracking data. Activities conducted while actively tracking through Cassini's high gain antenna (HGA), aligned along the spacecraft Z-axis, are utilized to calibrate and assess telemetry computations. Cassini's four uncoupled RCS thrusters are also aligned with the Z-axis, so ΔV is imparted along the spacecraft-to-Earth line and is directly observable in the X-band Doppler and range tracking data. Misalignments are negligible and ΔV magnitudes are easily reconstructed to within a few hundredths of a millimeter per second.

Three types of events are evaluated. Because of differing software algorithms and hardware usage, main engine maneuvers, RCS maneuvers, and non-maneuver ΔV activities are evaluated separately.

A. Main Engine Maneuvers

Maneuvers producing a ΔV greater than approximately 0.27 m/s are executed with Cassini's prime 440 N main engine. Starting from an Earth pointed attitude, which allows tracking and communications with ground stations on Earth, the angle required to orient the spacecraft thrust direction along the desired burn attitude is decomposed into a roll, yaw, and 0.9 degree "offset" turn. Separate roll and yaw turns are implemented instead of a single turn to ensure that thermal constraints are not violated. After these two turns are completed, the nominal ME thrust vector is aligned with the desired thrust vector in inertial space. The final 0.9° offset turn compensates for a small ME misalignment discovered in flight.[18] It aligns the flight estimated ME thrust vector with the desired thrust vector in inertial space, thereby circumventing the need for a flight software update. Approximately fifteen seconds before main engine ignition, Engine Gimbal Electronics (EGE) are actuated to pre-aim the main engine so that the thrust vector passes through the estimated spacecraft center of mass. After the main engine burn is terminated by the accelerometer, each turn is "unwound" in reverse order, returning the spacecraft to Earth-point. Up to five minutes of quiescent time is allocated after each turn to allow propellant to settle. This sequence of events is displayed, not to scale, in Fig. 1.

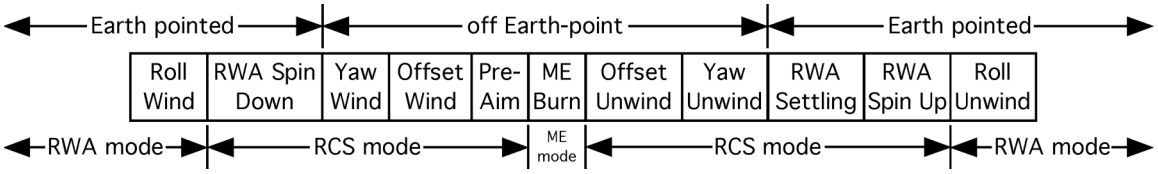

Figure 1. Sequence of events for main engine maneuver.

To preserve the health of the RWA, spinning reaction wheels are not subjected to the 440 N thruster force. After the roll wind turn and while the spacecraft is still pointed towards Earth, the spacecraft transitions to RCS mode and wheels are spun down to zero RPM. The spacecraft returns to Earth-point after completion of the yaw unwind turn, and after waiting 15 minutes for oscillations from the three Radio and Plasma Wave Subsystem (RPWS) antennas and Magnetometer boom to damp out (again to preserve the RWA health), reaction wheels are biased to a non-zero RPM and attitude control transitions back to RWA mode.

While the spacecraft is in RCS and ME modes, thrusting occurs from the 1 N and 440 N thrusters, respectively, and ΔV is imparted to the spacecraft. So long as the spacecraft remains on Earth-point and radio-metric tracking data are acquired, ΔV from each of the events is distinguishable and can be modeled separately. Because the RWA spin down and spin up occur on Earth-point, ΔV from these events is modeled separately from the ME burn. Yaw and offset turns occur off Earth-point, however, and cannot be distinguished from the ME burn with radio-metric tracking data. Therefore, Navigation Team estimates of ME maneuvers include the ΔV contribution from yaw and offset turns as well as any off Earth-point ΔV imparted while maintaining the spacecraft within deadband limitations. The portion of ΔV imparted to the spacecraft while in RCS mode is computed on-board according to Eq. (1). The portion imparted while in ME mode is computed according to Eq. (2). Spacecraft software simply sums ΔV computed in each RTI with the running total until a reset is encountered, neglecting the bias induced by the ME misalignment. Therefore, upon receipt of telemetry on the ground, the ME portion of the burn must be extracted, rotated to account for the ME misalignment, and then re-summed with the RCS portion of the burn. Because the misalignment is constant when defined relative to spacecraft coordinates, removal of the pointing bias is achieved by

rotating the ICRF main engine ΔV vector into spacecraft-fixed coordinates defined just prior to main engine ignition, applying the 0.9˚ rotation, and then rotating the resulting vector back to ICRF coordinates according to

$$\Delta \boldsymbol{V}_{unbiased} = \mathbf{ETOX}^{\mathrm{T}}\ \mathbf{R}^{\mathrm{T}}\ \mathbf{Y}^{\mathrm{T}}\ \mathbf{STOI}^{\mathrm{T}}\ \mathbf{TURN}\ \mathbf{STOI}\ \mathbf{Y}\ \mathbf{R}\ \mathbf{ETOX}\ \Delta \boldsymbol{V}_{biased} \tag{3}$$

ETOX is the transformation matrix from ICRF to spacecraft coordinates before implementation of the roll wind turn and is provided by the Cassini Attitude and Articulation Control Team (AACS). **R** and **Y** rotate the spacecraft coordinate system with the roll and yaw turns respectively, **STOI** rotates from spacecraft coordinates to an intermediate coordinate system where one axis is aligned with the anti-offset turn axis, and **TURN** rotates the vector by 0.9 degrees about the anti-offset turn axis. If ψ is the roll angle and θ the yaw angle and the z-axis of the intermediate coordinate system is chosen to be aligned with the anti-offset turn axis, then

$$\mathbf{R} = \begin{bmatrix} \cos\psi & \sin\psi & 0 \\ -\sin\psi & \cos\psi & 0 \\ 0 & 0 & 1 \end{bmatrix},\ \mathbf{Y} = \begin{bmatrix} \cos\theta & 0 & -\sin\theta \\ 0 & 1 & 0 \\ \sin\theta & 0 & \cos\theta \end{bmatrix},\ \text{and}\ \mathbf{TURN} = \begin{bmatrix} \cos(0.9°) & -\sin(0.9°) & 0 \\ \sin(0.9°) & \cos(0.9°) & 0 \\ 0 & 0 & 1 \end{bmatrix}$$

To complete a right-handed orthogonal coordinate system for the intermediate coordinate system, the x-axis can be chosen to lie along the cross product of the anti-offset turn axis and $\Delta \boldsymbol{V}_{biased}$ (they are never coincident), and the y-axis is then the cross product of the x- and z-axes.

All main engine maneuvers with telemetry resolution of 0.04 mm/s were included in this analysis. From OTM025, the first maneuver with high precision telemetry, to OTM156, the last reconstructed maneuver, there were fifty-six main engine maneuvers. The other 75 maneuvers were either performed in RCS mode or were canceled. Navigation estimates and uncertainties of this set of main engine maneuvers are provided in Table 1 along with telemetered values that have been adjusted to correct for the ME misalignment. Telemetered values have been converted from ICRF Cartesian coordinates to ICRF spherical coordinates, the coordinate system used in the finite burn model of JPL's Orbit Determination Program.

A maximum-likelihood estimator is applied to determine accuracies of magnitude, RA, and declination estimates derived from telemetry. First, differences between the navigation reconstruction and telemetry estimate are computed for each maneuver, or sample. RA differences and uncertainties must be normalized to account for variations with declination. Normalization is achieved by converting angular RA differences and uncertainties into subtended arc lengths (for small angles, this is accomplished by multiplying the RA difference or uncertainty by the cosine of the declination). Both navigation reconstructions and telemetry-based derivations of these quantities are assumed to have a Gaussian distribution, so the difference between estimates will also be Gaussian. Because the two estimation methods are independent, the uncertainty in the difference of the estimates for each sample may be derived as the RSS of the uncertainty from each method. Given these assumptions, the probability density function is defined as

$$f_m(x, \sigma_{ODP}, \sigma_{tel}) = \left[2\pi\left(\sigma_{ODP}^{\ 2} + \sigma_{tel}^{\ 2}\right)\right]^{-0.5} \exp\left[-\frac{1}{2}\left(x - \mu_m\right)^2\left(\sigma_{ODP}^{\ 2} + \sigma_{tel}^{\ 2}\right)^{-1}\right] \tag{4}$$

Uncertainties from the navigation reconstruction, σ_{ODP}, are readily available for each sample as an outcome of the orbit determination process. Uncertainties from the telemetry-based derivation are σ_{tel}, the desired quantities, and are assumed to be constant across all samples. x is the difference between the navigation reconstruction and telemetry-based maneuver parameter and μ_m is the mean, or bias, of the differences. The likelihood function is then defined as the product of evaluations of f_m for each measurement

$$L_m(\sigma_{tel}) = \prod_{i=1}^{N} f_m(x_i, \sigma_{ODP}, \sigma_{tel}) \tag{5}$$

Maximizing the likelihood function for each parameter (magnitude, normalized RA, and declination difference) provides an estimate of σ_{tel} for each of the three maneuver parameters. Results are listed in Table 2 where the value of σ_{tel} for RA is normalized. An un-normalized uncertainty for RA can be realized for each sample by dividing the normalized uncertainty by the cosine of the sample declination. In Fig. 2, differences between navigation reconstructions and telemetry computations for each ME maneuver are plotted with one-sigma error bars composed

of the RSS of σ_{ODP} and σ_{tel}. The percentage of data points within one-sigma of the mean difference are 71%, 75%, and 68% for magnitude, normalized RA, and declination, respectively, all near the 68% expected for a normal distribution. To further support the assumption of a normal distribution, maneuver samples are plotted against a Gaussian Cumulative Distribution Function (CDF) in Fig. 3. Deviations from the CDF are reasonable given the small number of samples.

Table 1. Main Engine Maneuver Estimates and Uncertainties.

Maneuver	Achieved ΔV From Telemetry (Corrected for ME misalignment)			Achieved ΔV From NAV Reconstruction					
				Mean			1-σ Uncertainty		
	Mag (mm/s)	RA (º)	Dec (º)	Mag (mm/s)	RA (º)	Dec (º)	Mag	RA (º)	Dec (º)
OTM025	351.88	246.309	-5.053	365.75	246.072	-5.591	0.30	0.147	0.415
OTM026	2616.62	37.678	20.473	2621.99	37.540	20.476	1.04	0.027	0.061
OTM027	2415.12	152.340	-57.704	2416.63	152.356	-57.730	1.36	0.015	0.009
OTM029	1448.80	74.009	-44.298	1452.78	74.048	-44.293	1.35	0.023	0.025
OTM030	14345.57	166.453	-57.125	14357.13	166.413	-57.153	0.92	0.003	0.002
OTM033	27904.12	193.100	7.240	27929.63	193.186	7.179	0.25	0.001	0.003
OTM038	14820.88	12.967	-10.342	14831.78	12.889	-10.264	0.09	0.001	0.002
OTM041	12408.55	22.747	-3.603	12422.80	22.646	-3.556	0.08	0.002	0.006
OTM042	2122.32	322.682	7.694	2126.24	322.645	7.673	0.21	0.018	0.013
OTM056	453.63	268.159	4.233	470.62	268.275	4.223	0.16	0.012	0.025
OTM057	350.81	126.919	-0.967	367.33	126.815	-0.894	0.07	0.026	0.020
OTM059	492.84	313.463	21.764	509.97	313.480	21.804	0.24	0.017	0.029
OTM063	1914.53	60.596	41.514	1916.00	60.570	41.524	0.09	0.003	0.003
OTM069	5415.37	352.175	61.304	5419.87	352.091	61.311	0.70	0.008	0.004
OTM071	6571.78	335.832	20.340	6583.50	335.781	20.403	1.92	0.010	0.026
OTM072	8164.38	332.922	56.196	8159.96	332.846	56.154	1.97	0.008	0.005
OTM075	6473.93	26.219	48.515	6473.72	26.188	48.543	0.18	0.001	0.001
OTM078	844.12	92.276	45.216	847.46	92.238	45.151	0.18	0.015	0.014
OTM080	3663.47	318.889	-24.939	3663.28	318.934	-24.914	0.06	0.003	0.002
OTM083	792.20	5.967	-6.451	791.40	5.962	-6.388	0.15	0.019	0.020
OTM084	6866.88	342.335	-1.250	6866.73	342.306	-1.242	0.06	0.001	0.001
OTM086	478.01	346.799	-18.321	495.29	346.744	-18.381	0.13	0.038	0.037
OTM087	1642.21	334.497	-20.218	1649.04	334.463	-20.240	0.05	0.007	0.005
OTM090	2390.24	318.704	-32.158	2394.69	318.733	-32.132	0.07	0.004	0.003
OTM093	269.26	222.587	-43.610	278.06	222.840	-43.687	0.26	0.032	0.063
OTM096	661.63	176.887	-2.881	663.95	176.944	-2.883	0.83	0.053	0.039
OTM098	1065.08	97.213	38.924	1074.58	97.173	38.861	0.28	0.027	0.082
OTM099	1611.42	202.783	-4.132	1611.82	202.853	-4.039	0.45	0.019	0.031
OTM101	525.72	78.817	38.256	540.56	78.831	38.478	0.38	0.027	0.231
OTM102	2693.23	201.987	9.428	2693.23	201.897	9.471	0.63	0.013	0.021
OTM105	3529.63	190.609	46.186	3532.39	190.647	46.176	0.26	0.005	0.006
OTM108	5580.28	201.124	61.630	5582.91	201.206	61.617	0.34	0.006	0.005
OTM111	5531.51	202.456	61.910	5533.99	202.511	61.888	0.22	0.004	0.003
OTM113	696.09	23.064	1.156	698.46	23.037	1.169	0.30	0.076	0.193
OTM114	12234.91	227.515	72.819	12235.67	227.688	72.777	1.39	0.007	0.002
OTM116	746.16	328.574	26.284	747.11	328.614	26.406	1.43	0.039	0.124
OTM117	7969.51	323.775	84.091	7969.60	323.326	84.062	1.17	0.027	0.002
JTM123	413.25	198.346	7.798	426.78	198.242	7.820	0.33	0.042	0.036
OTM125	473.50	159.133	39.152	487.96	159.196	39.230	0.70	0.064	0.150
OTM128	13480.28	311.698	65.126	13471.95	311.618	65.064	2.53	0.013	0.002
OTM131	1325.49	301.782	35.335	1327.14	301.810	35.418	0.59	0.026	0.026
OTM132	972.15	276.269	-49.006	977.19	276.182	-49.005	0.49	0.024	0.037
OTM134	1167.77	352.533	34.163	1172.68	352.755	34.181	0.45	0.050	0.025
OTM135	15755.37	281.891	62.610	15762.56	281.856	62.521	0.51	0.006	0.002
OTM137	678.29	193.487	12.043	680.89	193.504	12.145	0.25	0.025	0.036
OTM138	9635.88	254.223	74.284	9635.75	254.364	74.214	0.36	0.004	0.002
OTM141	2047.80	193.245	68.052	2046.45	193.310	68.050	0.18	0.018	0.007
OTM143	2875.28	129.422	-1.700	2878.60	129.443	-1.688	0.21	0.004	0.005
OTM144	37394.43	214.990	35.493	37406.25	215.078	35.432	0.20	0.000	0.000
OTM145	293.33	64.288	36.798	291.15	64.330	36.554	0.23	0.040	0.052
OTM146	7021.61	225.663	-44.737	7020.58	225.692	-44.798	0.22	0.003	0.003
OTM147	1115.67	338.455	74.256	1120.39	338.543	74.317	0.23	0.049	0.010
OTM149	2751.28	166.555	23.986	2752.83	166.595	24.001	0.25	0.011	0.005
OTM152	3321.57	345.942	21.647	3327.28	345.909	21.632	0.20	0.009	0.005
OTM153	502.74	330.785	-34.177	515.26	330.780	-34.126	0.21	0.053	0.034
OTM155	1166.96	339.225	26.174	1172.77	339.289	26.203	0.12	0.012	0.007

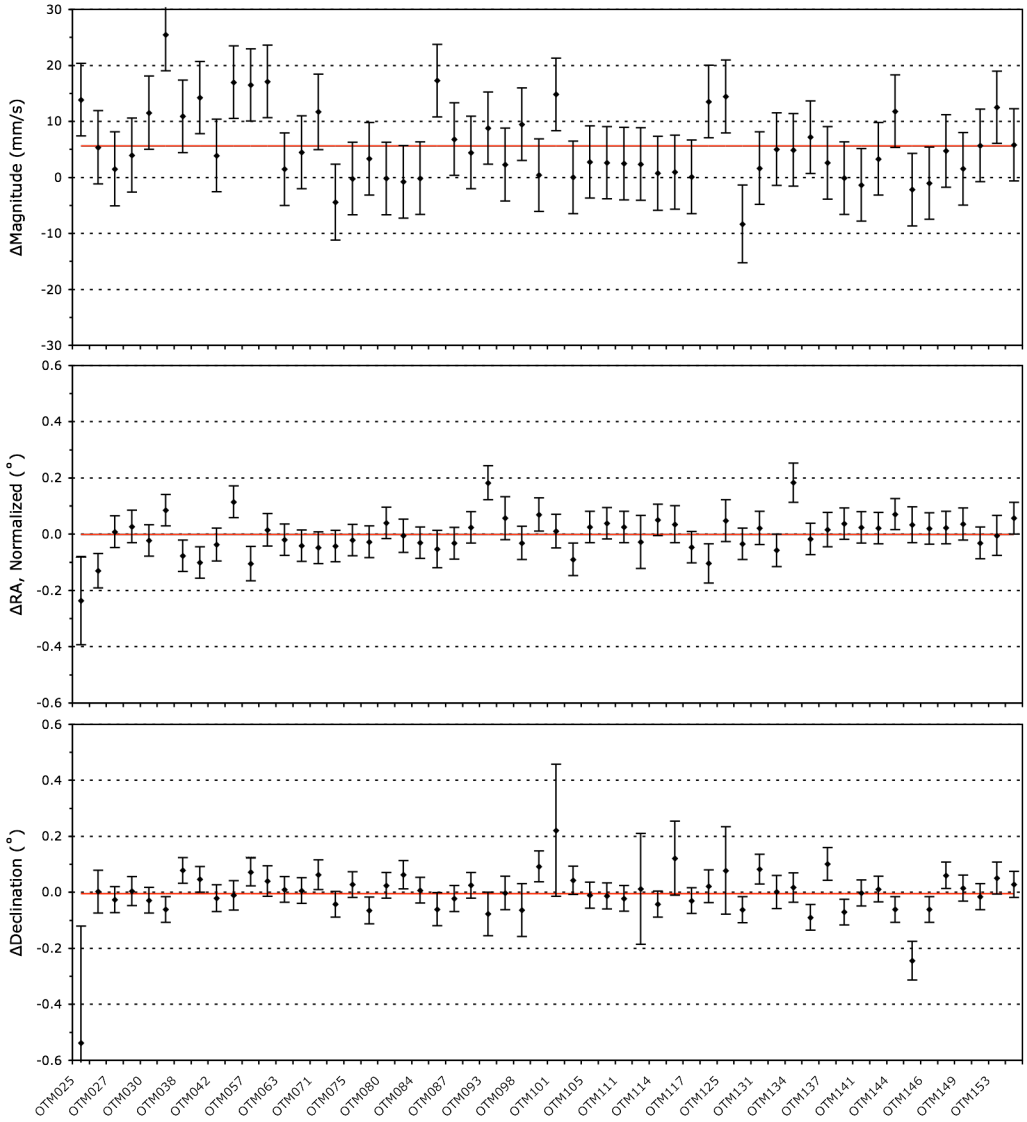

Figure 2. Main engine maneuver ΔV differences: navigation reconstruction minus telemetry computation. *Mean difference is red line.*

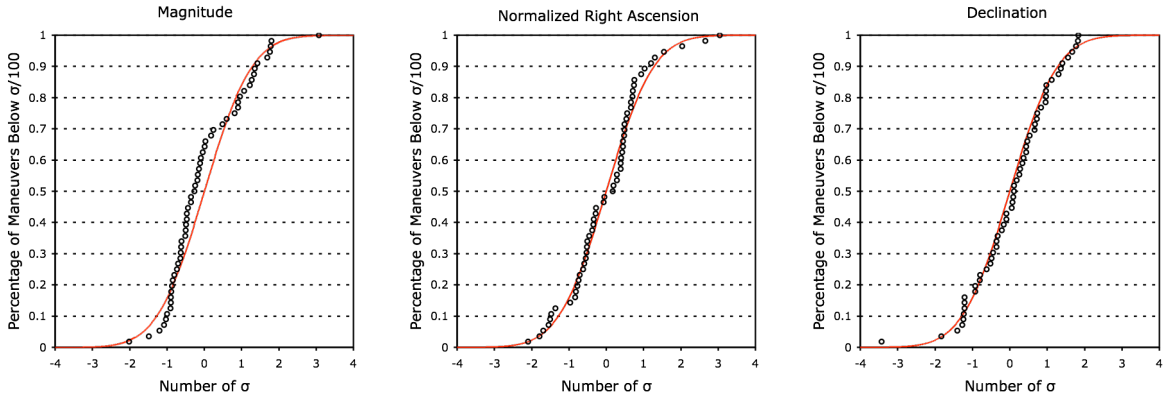

Figure 3. CDFs for main engine maneuver ΔV differences. *Samples are black circles, normal CDF is red line.*

Table 2. Biases and Telemetry Accuracies for Main Engine Maneuvers.

	Magnitude (mm/s)	Normalized Right Ascension (˚)	Declination (˚)
Bias (μ_m)	5.63	-0.001	-0.005
Telemetry uncertainty (σ_{tel})	6.47	0.056	0.046

With a bias of 5.6 mm/s, telemetry-based magnitude computations are significantly smaller than navigation reconstruction estimates. Biases of this size due to accelerometer calibration factors are not plausible because achieved ΔVs, terminated by accelerometer, are very close to commanded values. Nor is the bias contained within the ODP estimate, since for the overwhelming majority of ME maneuvers, ODP uncertainties are more than 10 times smaller. The bias is attributed to a systematic error in the telemetry record. Evidence of a telemetry magnitude bias may exist in the telemetry time-history record, where a decrement in maneuver magnitude is sometimes observed when the spacecraft transitions from ME mode after the main engine portion of the maneuver ends to RCS mode before the 0.9˚ offset unwind turn begins. The cause of the decrement across this boundary is currently not understood. Telemetry is typically recorded at two-second intervals during this phase of the maneuver (4 second intervals prior to OTM069). A higher record rate may provide further insight, but is not currently planned.

The one-sigma telemetry uncertainty of 6.47 mm/s is larger than the *a priori* uncertainty provided via the 2007-02 maneuver execution-error model for all maneuvers with a magnitude less than 20.5 m/s. Because only two of the 56 maneuvers included in the data set, OTM033 and OTM144, exceed this magnitude and because future maneuvers through the two-year extended mission[19] are all expected to be less than 20.5 m/s, telemetry-based magnitude information for ME maneuvers is not utilized in Cassini operations.

For maneuvers smaller than 3.9 m/s, telemetry-based pointing estimates are more accurate than *a priori* values provided by the 2007-02 maneuver execution-error model and are regularly utilized in Cassini operations. For maneuvers larger than 5.6 m/s, the 2007-02 model is more accurate and is not supplanted with the telemetry-based model. Between 3.9 and 5.6 m/s, the telemetry-based estimate is more accurate for declination, whereas the 2007-02 estimate is more accurate for right ascension. In both cases, pointing errors are assumed uncorrelated, so hybrid models are easily implemented. In Fig. 4, fixed telemetry-based one-sigma pointing uncertainties are superimposed onto a plot showing the 2007-02 errors as a function of maneuver magnitude. RA and declination biases between telemetry estimates and navigation are small compared to the one-sigma telemetry uncertainty and may be ignored.

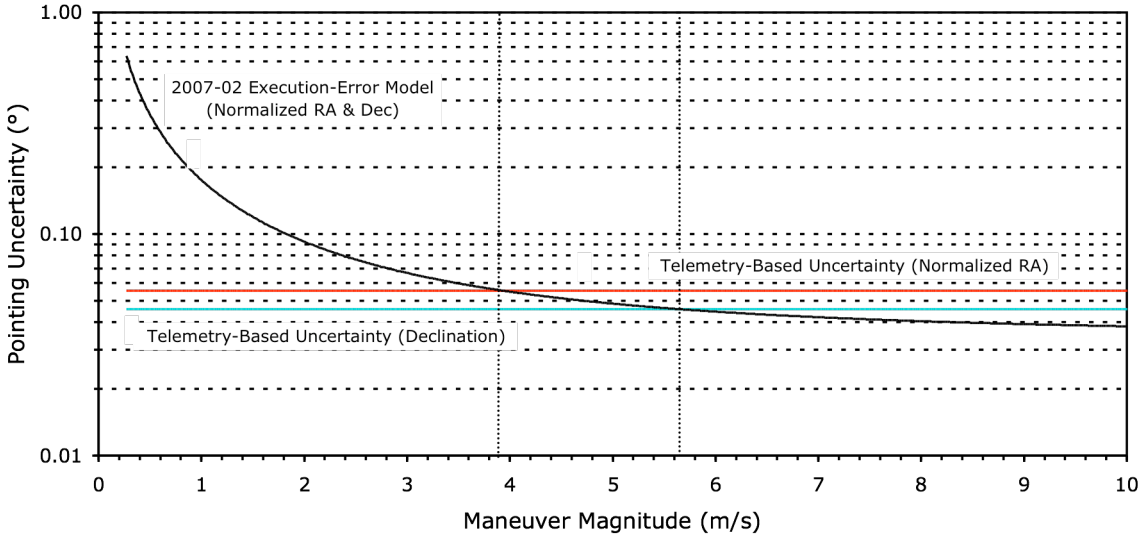

Figure 4. Main engine crossover points for determining usage of 2007-02 execution-error model vs. telemetry.

B. Reaction Control System Maneuvers

Maneuvers requiring a ΔV less than approximately 0.27 m/s are executed with Cassini's four 1 N *z*-axis facing thrusters. Starting once again from an Earth pointed attitude, the angle required to orient the spacecraft thrust direction along the desired burn attitude is decomposed into a roll and yaw turn. In contrast to ME burns, all RCS maneuver turns are implemented with reaction wheels, so ΔV is not imparted to the spacecraft. Fifteen seconds

before burn ignition, attitude control deadbands are loosened to 8.7 mrad about the *x*- and *y*-axes and 17.5 mrad about the *z*-axis in preparation for an imminent transition to RCS mode. Reaction wheels remain powered up and spinning, but control of attitude is transferred to thrusters. Two minutes after burn termination by the virtual accelerometer, spacecraft deadbands are tightened from (8.7, 8.7, 17.5) mrad to (2, 2, 2) mrad in preparation for a transition back to RWA mode. Turns are unwound in reverse order to return the spacecraft to Earth-point so that maneuver telemetry can be downlinked and tracking can resume. Reaction wheels are then biased to speeds that will maintain them within a safe operating regime through future anticipated turns. This sequence of events is displayed, not to scale, in Fig. 5.

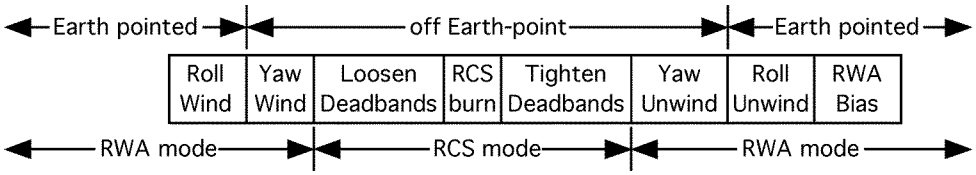

Figure 5. Sequence of events for reaction control system maneuver.

Although no ΔV is imparted to the spacecraft during RCS maneuver turns, the RCS burn is not the sole source of ΔV activity. After burn termination, a significant amount of thruster firing is required to remain within commanded deadband limits. In addition, a ΔV of a few millimeters per second is observed when deadband limits are tightened to 2 mrad per axis. As with ME burns, Navigation Team estimates of RCS maneuvers include all ΔV activity imparted to the spacecraft while it is off Earth-point. Because all thrusting occurs in RCS mode, telemetry estimates of ΔV activity are governed by Eq. (1).

All RCS maneuvers with telemetry resolution of 0.04 mm/s, 35 in all, were included in this analysis. Navigation estimates and uncertainties of this set of Reaction Control System maneuvers are provided in Table 3 along with telemetered values that have been converted to ICRF magnitude, RA, and declination coordinates.

As with ME burn processing, the maximum-likelihood estimator based on Eqs. (4) and (5) is applied to determine accuracies of RA and declination estimates derived from telemetry. Results are listed in Table 4 where the value of σ_{tel} for RA is again normalized. These uncertainties indicate that telemetry-based RA and declination estimates are three and four times more accurate respectively than *a priori* values provided by the 2007-02 maneuver execution-error model. Biases between telemetry estimates and navigation reconstructions are small compared to the one-sigma telemetry uncertainty and may be ignored. In Fig. 6, differences between navigation reconstructions and telemetry computations for each RCS maneuver are plotted with one-sigma error bars composed of the root-sum-square of σ_{ODP} and σ_{tel}. The percentage of data points within one-sigma of the mean difference is 74% for both normalized RA and declination. Maneuver samples are overlaid upon a Gaussian CDF in Fig. 7.

Because the burn is terminated via a virtual accelerometer, or timer, instead of an actual accelerometer, magnitude estimates are always equivalent to commanded values. I.e., the burn is terminated when the telemetry computation of ΔV magnitude computed from Eq. (1) achieves the commanded ΔV magnitude value. Of course, the actual ΔV will differ from telemetered and commanded ΔV's because the on-board thrust values, which vary with burn duration, propellant tank pressure, and propellant temperature, are not perfectly known. So telemetry magnitude computations cannot be used in the same manner as for ME burns. Instead, telemetry magnitude estimates are utilized to determine the approximate amount of post-burn ΔV imparted to the spacecraft from deadband cycling and tightening of deadband limits. Because this thrusting occurs before unwind turns are executed, the ΔV is directed along the burn attitude. Samples of post-burn ΔV are gathered and statistically analyzed to enable a prediction of future post-burn ΔV magnitudes. This prediction is then factored into RCS maneuver designs to prevent systematic errors in the overburn direction.

Two methods are implemented and compared to determine the approximate amount of post-burn ΔV imparted to the spacecraft. Methods differ in the thrust quantity applied to post-burn thrusting. Method 1 scales telemetered post-burn ΔV by the ratio of the navigation reconstruction estimate to the telemetered computation of the entire off-Earth-pointed ΔV. It assumes that the post-burn thrust force is equivalent to the average force over the off-Earth-pointed activity. Method 2 scales telemetered post-burn ΔV by the ratio of thrust determined from the Earth pointed RWA bias immediately following the maneuver to the on-board thrust value. It assumes the post-burn thrust force is equivalent to the force determined from the RWA bias activity. Fig. 8 is a plot of post-burn ΔV computed from each of these methods. An analysis of all samples using method 1 yields an estimate of 4.47±0.55 mm/s (1-σ). Method 2 yields a statistically equivalent estimate of 4.51±0.54 mm/s. Limitations imposed by the 2 or 4 second telemetry sampling interval prevent a reliable allocation of telemetered ΔV between burn and post-burn events during the

interval when the burn terminates. RCS maneuvers are generally designed assuming that 4.5 mm/s of post-burn ΔV directed along the burn attitude will be present.

Table 3. Reaction Control System Maneuver Estimates and Uncertainties.

Maneuver	Achieved ΔV From Telemetry			Achieved ΔV From NAV Reconstruction					
				Mean			1-σ Uncertainty		
	Mag (mm/s)	RA (º)	Dec (º)	Mag (mm/s)	RA (º)	Dec (º)	Mag	RA (º)	Dec (º)
OTM031	63.14	109.068	11.696	64.37	108.772	11.222	0.08	0.152	0.501
OTM035	293.98	28.187	-5.606	296.20	28.026	-5.592	0.46	0.040	0.077
OTM039	89.87	223.218	-7.339	91.33	223.436	-7.073	0.43	0.150	0.293
OTM043	59.56	248.337	11.309	60.44	248.606	11.390	0.24	0.194	0.479
OTM044	236.71	4.674	-18.993	240.87	4.596	-19.174	0.10	0.036	0.101
OTM047	183.00	64.782	67.244	181.62	64.540	67.067	0.15	0.068	0.077
OTM051	186.17	56.275	-28.587	185.18	56.249	-28.757	0.21	0.021	0.039
OTM053	265.72	234.709	24.653	263.24	234.879	24.780	0.12	0.014	0.027
OTM058	77.43	70.316	-4.533	78.64	70.168	-4.650	0.09	0.060	0.160
OTM061	120.16	170.217	4.295	122.09	170.433	4.500	0.23	0.151	0.383
OTM064	69.19	221.505	26.028	69.73	221.706	26.211	0.17	0.061	0.128
OTM065	136.51	134.400	39.441	137.87	134.297	39.652	0.10	0.070	0.101
OTM070	227.60	148.615	15.755	227.51	148.797	15.844	0.07	0.144	0.454
OTM076	40.23	143.308	33.696	41.01	142.893	33.731	0.12	0.459	0.490
OTM079	62.90	137.594	31.305	63.68	137.058	30.891	0.13	0.355	0.369
JTM081	220.23	123.892	44.281	220.30	123.527	44.202	0.05	0.051	0.046
OTM088	41.27	317.394	-31.428	42.05	317.519	-32.139	0.07	0.418	0.340
OTM089	212.99	327.720	-41.857	213.06	327.387	-41.665	0.10	0.053	0.050
OTM091	14.69	117.567	33.358	14.96	117.469	33.146	0.06	0.505	0.447
OTM094	40.76	231.923	-34.009	41.40	232.251	-33.186	0.17	0.076	0.205
OTM100	69.13	135.353	-37.078	69.51	135.628	-37.083	0.20	0.281	0.119
OTM103	37.38	151.091	-10.667	37.78	151.400	-10.674	0.07	0.378	0.306
OTM106	16.71	195.966	24.006	17.17	196.039	24.139	0.17	0.480	0.447
OTM109	24.93	262.796	-29.515	25.31	262.824	-29.431	0.14	0.261	0.515
OTM115	36.19	161.261	62.551	36.68	161.820	62.799	0.35	0.565	0.449
OTM118	12.88	150.322	-4.274	13.25	150.565	-4.280	0.05	0.426	0.515
OTM119	23.95	121.021	-30.073	24.11	121.601	-29.855	0.16	0.404	0.346
OTM121	13.29	61.968	-2.415	12.87	62.178	-2.356	0.66	0.284	0.500
OTM129	102.99	64.983	-46.027	102.96	64.889	-46.366	0.87	0.161	0.433
OTM130	24.19	289.061	64.513	23.88	289.254	64.181	0.52	0.648	0.391
OTM133	67.39	244.991	-4.562	67.47	245.104	-4.341	0.23	0.081	0.418
OTM136	19.25	188.586	16.168	19.38	187.514	16.283	0.08	0.482	0.502
OTM139	13.39	130.960	55.262	13.62	131.290	54.997	0.11	0.726	0.476
OTM150	54.82	192.244	-38.651	55.24	192.483	-38.667	0.12	0.173	0.126
OTM156	197.34	164.657	-11.742	195.83	165.035	-11.718	0.04	0.057	0.036

Table 4. Biases and Telemetry Accuracies for Reaction Control System Maneuvers.

	Normalized Right Ascension (˚)	Declination (˚)
Bias (μ_m)	0.028	-0.005
Telemetry uncertainty (σ_{tel})	0.171	0.137

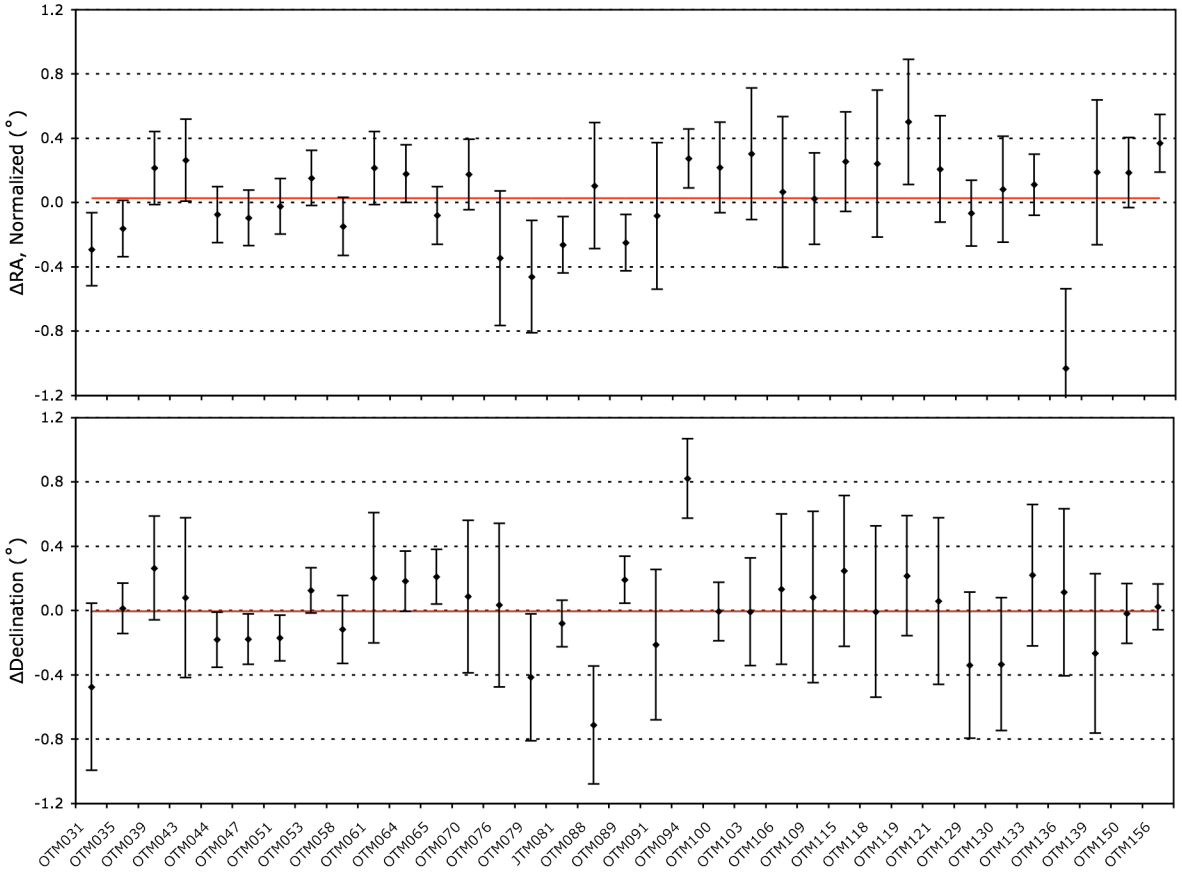

Figure 6. Reaction control system maneuver ΔV differences: navigation reconstruction minus telemetry computation. *Red line is mean difference.*

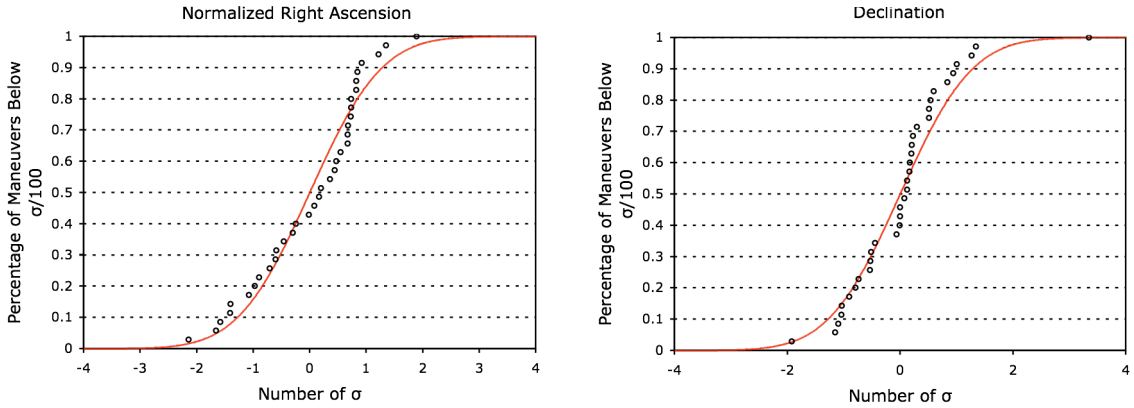

Figure 7. CDFs for reaction control system maneuver ΔV differences. *Normalized right ascension and declination samples (black circles), normal CDF (red line).*

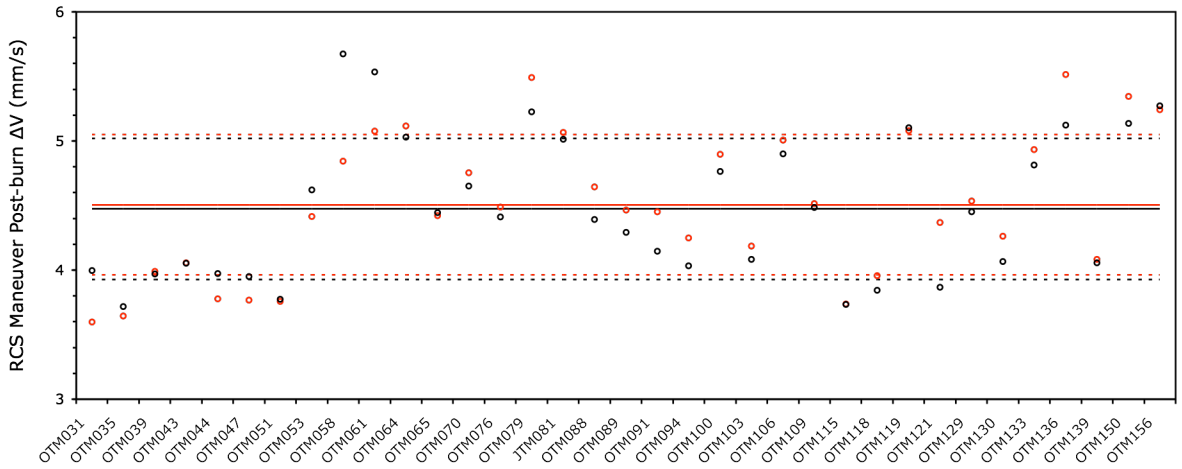

Figure 8. Reaction control system maneuver post-burn ΔV. *Average thrust method (black), RWA bias thrust method (red). Dashed lines are 1-σ error bars. Solid lines are mean estimate.*

C. Non-Maneuver ΔV Activities

Non-maneuver ΔV activities include thrusting events necessary to maintain the health and safety of reaction wheels and to enable, enhance, and expand science observations. RWA biases are routinely performed to manage spacecraft momentum and thereby maintain reaction wheels within a safe operating regime. Friction tests are performed quarterly to monitor the health of Cassini's three operational reaction wheels and semiannually to monitor the health of one additional redundant wheel. Science observations are enabled by transitioning to RCS mode near selected satellite encounters, allowing faster turn rates to accumulate more observations and greater control authority to cancel drag induced torques during low altitude flybys. Observations from at least one science instrument, the Radio and Plasma Wave Science instrument, are enhanced by transitioning to RCS mode for 4 hour intervals near many Saturn periapsis passages.

Similar to RCS maneuvers, non-maneuver ΔV computations are governed by Eq. (1). In contrast to RCS maneuvers, however, activities are not terminated by the virtual accelerometer and meaningful magnitude information is obtainable. Before these computations can be included into the navigation process, thrust must be calibrated. Calibration is accomplished by rearranging Eq. (1) to solve for thrust using navigation estimates of well-determined ΔV's. The calibration process is ongoing because thrust decreases as propellant is expended and tank pressure decreases. The navigation thrust computation is compared to values obtained from a propulsion model based on tank pressure, temperatures, and propellant mass. In Fig. 9, the "stair step" line represents propulsion estimates of thrust, where estimates are typically adjusted after pressure changes of at least one DN are observed in telemetry. Black circles represent navigation estimates of thrust for each ΔV event. The scatter is caused by a variety of reasons, including errors in the navigation estimate, varying thruster duty cycles, thruster cluster temperature increases for the larger ΔV's, and variations in tank temperature caused by bus heater switches. Occasionally, navigation estimates may begin to deviate from the propulsion model, causing re-examination of all models. Previously, deviations provided evidence for adjusting thruster tail-off time constants[14], a second-order effect that was confirmed upon examination of pre-launch test data at varying tank pressures. The adjustment was made just prior to the first circle from the data set shown in Figure 9.

An assessment of pointing accuracies based on this data set was not performed since navigation pointing is not typically well determined for small ΔV's such as these. Pointing accuracies are assumed to be somewhat worse than those described in the previous discussion of RCS maneuvers because the telemetry resolution is a larger percentage of the ΔV. Pointing errors are expected to be within approximately 1°.

Differences between propulsion and navigation estimates of thrust, expressed as a percentage of the total navigation estimate are shown in Figure 10. If we assume that the total uncertainty is the RSS of the navigation uncertainty and propulsion model uncertainty, and if the latter is 1.7%, the maximum-likelihood estimator places 67% of the samples within one standard deviation of the mean (-0.07%). As an interesting side note, the standard deviation of the plotted data set (assuming perfect navigation estimates) is 1.8%, demonstrating that the majority of the uncertainty is within the propulsion model. Rounding up, constraints applied in the navigation process for ΔV activity performed without benefit of Doppler tracking coverage should be at least 2% of the total telemetry computations of ΔV after scaling to account for mismatches between the on-board thrust value and the propulsion estimate.

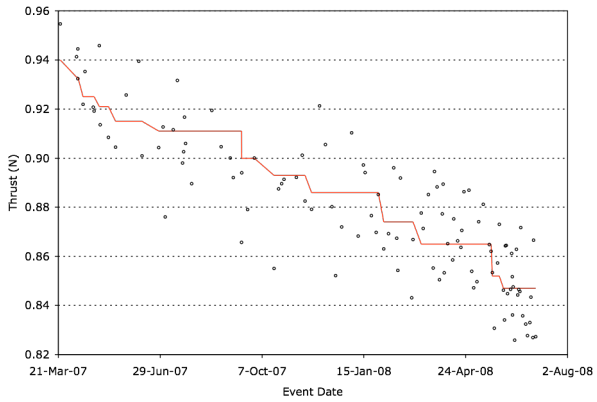

Figure 9. Thruster force estimates. *Propulsion estimate (red line), navigation reconstruction (black circles).*

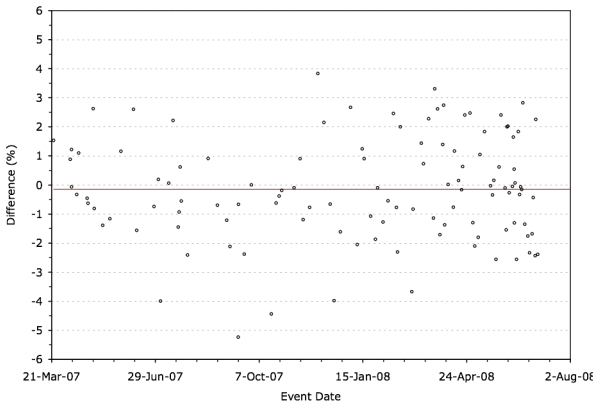

Figure 10. Thruster percentage differences: navigation reconstruction minus propulsion estimate. *Red line is mean difference.*

IV. Benefit to Cassini Navigation

Calibrated ΔV telemetry is potentially ten times more accurate than *a priori* ME maneuver models and is three to four times more accurate than *a priori* RCS maneuver models. It also provides a more accurate estimate of non-maneuver ΔV activities executed in the blind, a phenomenon that is becoming more frequent as efforts to maintain the health of reaction wheels are emphasized. The on-board computations become available to the Navigation Team within a few hours of maneuver executions, which are nominally scheduled over tracking passes, and near the beginning of the first pass following those ΔV activities executed in the blind. Upon inclusion of telemetry models into the orbit determination process, both orbit predictions and reconstructions are improved.

Considering the rather large knowledge improvement over *a priori* maneuver models, there is a temptation to conclude that targeting accuracies are also vastly improved. In fact, targeting accuracy improvements are generally minimal, as the interval between maneuvers is usually sufficient to allow radio-metric and optical tracking data types to re-converge the trajectory estimate to a comparable level with or without telemetry by the time of the final tracking data cutoff. In the few rare cases when targeting accuracies are significantly improved with utilization of telemetry (where, for example, unfavorable orbit geometries cannot be well determined with tracking data or near solar conjunctions when tracking data are considerably noisier) target misses can be reduced, thereby reducing downstream ΔV expenditures and improving science instrument pointing.

The primary benefit maneuver ΔV telemetry brings to the navigation process is rapid convergence of trajectory estimation. Convergence levels typically obtained in a matter of days with tracking data can be obtained in a matter of hours with telemetry, leading to more stable designs of the next maneuver. The maneuver design and review process is intentionally spread over several days to ensure design maturity, with updates performed after additional tracking passes are obtained. As additional tracking data are acquired and processed, smaller deviations in orbit predictions are observed, instilling confidence in the orbit solutions. Variations between maneuver design updates are smaller, allowing for quicker identification and more thorough discussion of potential design issues and options such as constraint violations, execution mode (RCS or ME) for borderline magnitudes, maneuver biasing, maneuver cancellation, and turns resulting in undesirable momentum transfer between reaction wheels.

One of the more pronounced examples of orbit convergence improvement is shown in Figure 11, where orbit determination relying on the 2007-02 *a priori* execution error model is compared to the telemetry-based model. Orbit estimates and one-sigma error ellipses mapped to the B-plane of the next targeted Titan encounter are shown for a progression of tracking data cutoffs. For the 2007-02 solutions, data cutoffs are advanced to the end of each successive pass after the 6 April 2006 execution of OTM057 (labels indicate data cutoffs). As data cutoffs progress, the 2007-02 based mean estimate gradually shifts downward and to the right as error ellipses shrink, converging around the Titan 13 reconstructed solution (error ellipse too small to be seen at scale of Fig. 11) approximately one week later. In contrast, telemetry-based solutions immediately converge around the reconstructed solution and corresponding error ellipses are much smaller. Reconstructed orbit solutions are not propagated beyond the tracking data and are the best available estimates of orbit arcs.

The primary benefit non-maneuver ΔV telemetry brings to the navigation process is improved modeling of satellite flybys conducted in RCS mode, both for predicted and reconstructed orbits. Prior to utilizing ΔV telemetry,

the absence of tracking data during ΔV activities clustered near closest approach entailed a tremendous effort to model RCS flybys, and large uncertainties remained afterwards. Orbit determination results supporting the flyby cleanup maneuver, usually scheduled three days after the flyby, were less accurate. For Titan flybys below an altitude of 1300 km, RCS mode is required to counter spacecraft torques induced by Titan's thick atmosphere. Telemetry computations of ΔV allow thrust induced ΔV activity to be modeled separately so that all remaining ΔV activity can be attributed to atmospheric drag.[20] An estimate of Titan's atmospheric density is the result, supplementing a primary science objective with an estimate derived independently from science instrumentation.

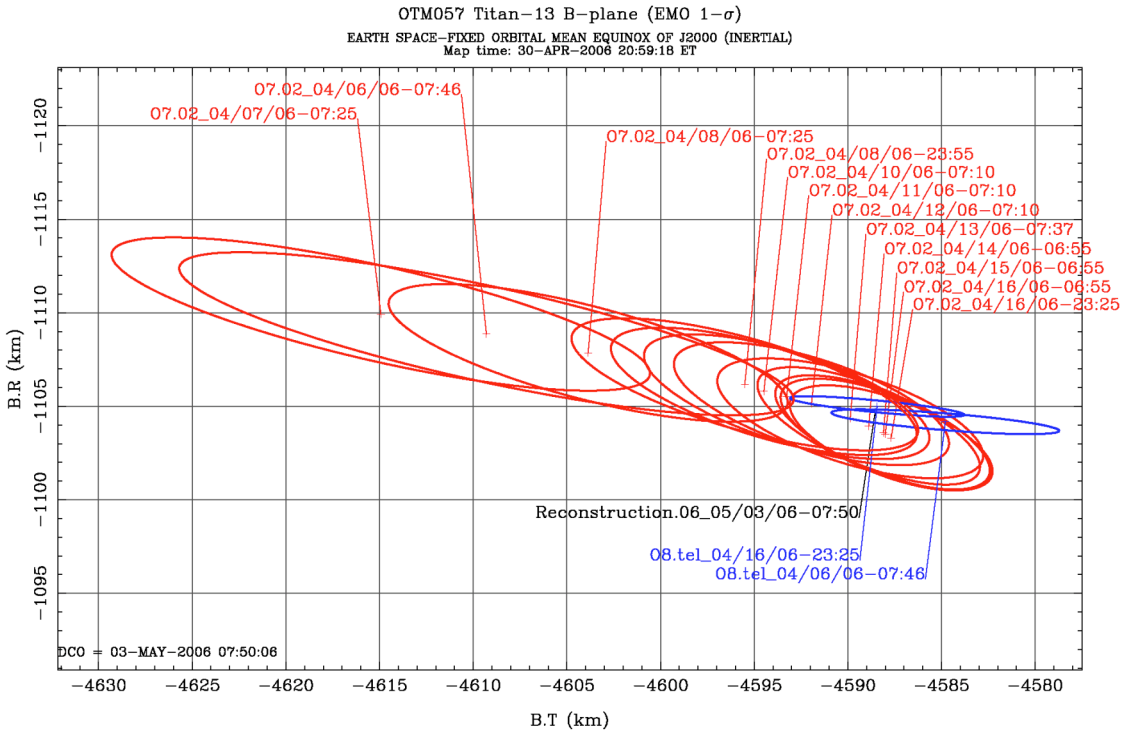

Figure 11. Orbit convergence comparison. *2007-02 model (red) vs. telemetry-based model (blue).*

Whereas the majority of the previous discussion centered on improvements to orbit predictions, orbit reconstruction accuracies can also be improved. Even though tracking data are available throughout a reconstructed arc, reconstructed maneuver pointing parameter uncertainties are sometimes larger than the uncertainties listed in Tables 2 and 4 if telemetry results are neglected. Several examples of this are apparent after normalizing the RA uncertainty and comparing the last two columns of Tables 1 and 3, where telemetry computations of ΔV were intentionally ignored, to the Table 2 and 4 uncertainties. Archival reconstructions delivered to the Cassini project since the Titan 13 encounter take advantage of ΔV telemetry, with constraints generally growing tighter as the telemetry evaluation matures. Because of workforce limitations, there are currently no plans to reprocess previously delivered reconstructions. Future archival reconstructions will implement the constraints listed in Tables 2 and 4 until further updates become available with the inclusion of future maneuvers to the data set.

Besides improving navigation accuracies, ΔV computations from telemetry also provide insight into burn characteristics. Monitoring these characteristics for unexpected changes can provide an early indication of adverse changes to flight hardware and operability or indicate that a parameter update is needed. Thrust associated with the tightening of AACS deadbands after RCS burns is routinely monitored to ensure that the 4–5 mm/s of ΔV is imparted to the spacecraft. Deviations of navigation estimates of RCS thrust from a Cassini propulsion model have already led to updates of the thruster tail-off time constant.

V. Conclusion

With the end of Cassini-Huygens' prime mission on July 1, 2008, Cassini has completed 58 targeted flybys and performed 131 of 186 planned maneuvers. Forty-three maneuvers were executed in RCS mode, 88 were executed in ME mode, and 55 were cancelled. Ample future opportunities exist to realize the benefits provided by telemetry computations of ΔV. Enough propellant remains on-board to impart approximately 350 m/s more ΔV to the

spacecraft. The Cassini Equinox extended mission, approved by NASA in spring 2008, begins when the prime mission ends, continues through fiscal year 2010, and will deplete a portion of the remaining propellant. Nominally requiring 220 m/s of propellant, the Equinox mission includes 32 more targeted flybys accomplished via execution of 95 additional scheduled maneuvers. Approximately 130 m/s of available ΔV capability is anticipated upon completion of the Equinox mission, leaving open the possibility of another mission extension. Future telemetry computations of ΔV will continue to be compared to navigation estimates of ΔV, providing additional samples from which the telemetry accuracy will be periodically re-assessed.

Most of the discussion of accuracy improvements has focused on localized spacecraft trajectory improvements, referring to tighter accuracies within only the trajectory arc containing the maneuvers. Global accuracy improvements are also realized because better local estimates of the spacecraft ephemeris translate into better estimates of quantities such as satellite ephemerides and Saturn and satellite gravity fields. In essence, as the local spacecraft ephemeris becomes more tightly constrained, the information content of radio-metric and optical tracking data serves to better determine Saturn system parameters. Improved estimates of Saturn system parameters then enable better reconstructions of all downstream spacecraft ephemeris reconstructions. They also supplement, enable, and improve science observations. Determination of a body's gravity field provides clues to its formation and interior composition. Satellite ephemeris improvements have enabled precision stellar occultations by Enceladus to determine the chemical composition and bound the density of its volcanic plumes and by Iapetus to determine if it has an atmosphere. They have also reduced science instrument pointing uncertainties. Radio occultations by the atmospheres of Saturn and Titan are especially sensitive to pointing errors, with half-power, half-beamwidth losses of the downlink Ka-band signal for pointing errors of 1.5 mrad.

Finally, improvements to Saturn system parameter estimates resulting from the inclusion of ΔV telemetry into the navigation process will also benefit future missions to Saturn. Titan and Enceladus flagship missions have recently been proposed.[21, 22]

Acknowledgments

The authors thank Jay Brown, Thomas Burk, and Peter Meakin of the Cassini AACS team for helpful discussions concerning on-board ΔV computation algorithms and OTM block sequence of events. The research described in this publication was carried out at the Jet Propulsion Laboratory, California Institute of Technology, under a contract with the National Aeronautics and Space Administration. Copyright 2008 California Institute of Technology. Government sponsorship acknowledged.

References

[1]Smith, J. C., "Description of Three Candidate Cassini Satellite Tours," AAS/AIAA Space Flight Mechanics Meeting, AAS 98-106, Monterey, California, 9-11 February 1998.

[2]Strange, N. J., Goodson, T. D., Hahn, Y., "Cassini Tour Redesign for the Huygens Mission," AIAA/AAS Astrodynamics Specialist Conference, AIAA 2002-4720, Monterey, California, 5-8 August 2002.

[3]Buffington, B., Strange, N., Smith, J., "Overview of the Cassini Extended Mission Trajectory," AIAA/AAS Astrodynamics Specialist Conference, AIAA 2008-6752, Honolulu, Hawaii, 18-21 August 2008.

[4]Lange, R. D., "Cassini-Huygens Mission Overview and Recent Science Results," IEEE Aerospace Conference, IEEEAC paper #1598, Big Sky, Montana, 1-8 March 2008.

[5]Antreasian, P. G., et. al., "Cassini Orbit Determination Performance During the First Eight Orbits of the Saturn Satellite Tour," AAS/AIAA Astrodynamics Specialist Conference, AAS 05-312, Lake Tahoe, California, 7-11 August 2005.

[6]Antreasian, P. G., et. al., "Cassini Orbit Determination Performance During Saturn Satellite Tour August 2005 – January 2006," AAS/AIAA Astrodynamics Specialist Conference, AAS 07-253, Mackinac Island, Michigan, 19-23 August 2007.

[7]Antreasian, P. G., et. al., "Cassini Orbit Determination Performance During Saturn Satellite Tour from January 2006 to January 2008," AIAA/AAS Astrodynamics Specialist Conference, AIAA-2008-6747, Honolulu, Hawaii, 18–21 August 2008.

[8]Wagner, S., V., et. al., "Cassini-Huygens Maneuver Experience: First Year of Saturn Tour," AAS/AIAA Astrodynamics Specialist Conference, AAS 05-287, Lake Tahoe, California, 7-11 August 2005.

[9]Wagner, S. V., et. al., "Cassini-Huygens Maneuver Experience: Second Year of Saturn Tour," AIAA/AAS Astrodynamics Specialist Conference, AIAA-2006-6663, Keystone, Colorado, 21-24 August 2006.

[10]Williams, P. N., et. al., "Cassini-Huygens Maneuver Experience: Third Year of Saturn Tour," AAS/AIAA Astrodynamics Specialist Conference, AAS 07-254, Mackinac Island, Michigan, 19-23 August 2007.

[11]Goodson, T. D., et. al., "Cassini-Huygens Maneuver Experience: Ending the Prime Mission," AIAA/AAS Astrodynamics Specialist Conference, AIAA-2008-6751, Honolulu, Hawaii, 18-21 August 2008.

[12]Roth, D. C., et al., "Cassini Tour Navigation Strategy," AAS/AIAA Astrodynamics Specialist Conference, AAS 03-546, Big Sky, Montana, 3-7 August 2003.

[13]Ma, C., et al., "The International Celestial Reference Frame as Realized by Very Long Baseline Interferometry," The Astronomical Journal, Vol. 116, July 1998, pp. 516-546.

[14]Ardalan, S. M., et al., "Integration of Spacecraft Telemetry into Navigation Operations for the Cassini-Huygens Mission," SpaceOps 2008 Conference, AIAA-2008-3412, Heidelberg, Germany, 12-16 May 2008.
[15]Bates, D., Lee, A., "In-flight Characterization of the Cassini Spacecraft Attitude Control Thrusters," AIAA Guidance, Navigation and Control Conference, AIAA 2007-6342, Hilton Head, South Carolina, 20-23 August 2007.
[16]Feldman, A., Lee, A., "In-flight Estimations of Cassini Spacecraft Inertia Tensor and Thruster Magnitude," AAS/AIAA Space Flight Mechanics Conference, AAS 06-102, Tampa, Florida, 22-26 January 2006.
[17]Wagner, S. V., Goodson, T. D., "Execution-Error Modeling and Analysis of the Cassini-Huygens Spacecraft Through 2007," AAS/AIAA Space Flight Mechanics Winter Meeting, AAS 08-113, Galveston, Texas, 27-31 January 2008.
[18]Goodson, T. D., Gray, D. L., Hahn, Y., Peralta, F., "Cassini Maneuver Experience: Finishing Inner Cruise," AAS/AIAA Space Flight Mechanics Meeting, AAS 00-167, Clearwater, Florida, 23-26 January 2000.
[19]Buffington, B., Strange, N., Smith, J., "Overview of the Cassini Extended Mission Trajectory," AIAA/AAS Astrodynamics Specialist Conference, AIAA-2008-6752, Honolulu, Hawaii, 18–21 August 2008.
[20]Pelletier, F. J., et al., "Atmospheric Drag Model for Cassini Orbit Determination During Low Altitude Titan Flybys," AAS/AIAA Space Flight Mechanics Conference, AAS 06-141, Tampa, Florida, 22-26 January 2006.
[21]Razzaghi, A. I., et al., "Enceladus Flagship Mission Concept Study," NASA Goddard Space Flight Center, 29 August 2007.
[22]Leary, J. C., et al., "Titan Explorer Flagship Mission Study," The Johns Hopkins University of Applied Physics Laboratory, January 2008.